ACS APPLIED MATERIALS & INTERFACES

Research Article

www.acsami.org

Preparation and Characterization of Microporous Layers on Titanium by Anodization in Sulfuric Acid with and without Hydrogen Charging

Shin-ichi Tanaka,*[,†] Yuriko Fukushima,[‡] Isao Nakamura,[§] Toshiyuki Tanaki,[§] and Gregory Jerkiewicz*[,∥]

[†]Department of Material Science and Engineering, Kurume National College of Technology, 1-1-1, Komorino, Kurume, Fukuoka 830-8555, Japan

[‡]Advanced Engineering School, Kurume National College of Technology, 1-1-1, Komorino, Kurume, Fukuoka 830-8555, Japan

[§]Tokyo Metropolitan Industrial Technology Research Institute, 1-20-20, Minami-Kamata, Ota-ku, Tokyo 144-0035, Japan

[∥]Department of Chemistry, Queen's University, 90 Bader Lane, Kingston, Ontario, K7L 3N6, Canada

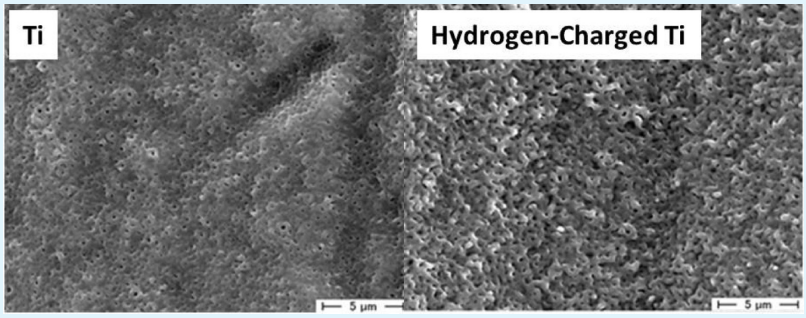

ABSTRACT: The formation of microporous oxide layers on titanium (Ti) by anodization in sulfuric acid (H_2SO_4) solution and the influence of prior hydrogen charging on their properties are examined using electrochemical techniques, scanning electron microscopy, grazing incident X-ray diffraction, and X-ray photoelectron spectroscopy. When Ti is anodized in 1 M aqueous H_2SO_4 solution at a high direct current (DC) potential (>150 V) for 1 min, a porous surface layer develops, and the process takes place with spark-discharge. Under these conditions, oxygen evolution at the Ti electrode proceeds vigorously and concurrently with the formation of anodic oxide. The oxygen gas layer adjacent to the Ti surface acts as an insulator and triggers spark-discharge; the latter stimulates the development of pores. In the absence of spark-discharge, the oxide layer has extended surface roughness but low porosity. A porous oxide layer can be prepared by applying a lower DC voltage (130 V) and without spark-discharge, but Ti requires prior hydrogen charging by cathodic polarization in 1 M aqueous H_2SO_4 solution. Mott–Schottky measurements indicate that the oxide layers are n-type semiconductors and that the charge carrier density in the anodic oxide layer on the hydrogen-charged Ti is lower than in the case of untreated Ti. The hydrogen charging also affects the flat band potential of the anodic oxide layers on Ti by increasing its value. The reduced charge carrier density brought about by hydrogen charging decreases the oxide layer conductivity and creates favorable conditions for its electrical breakdown that stimulates the development of pores. The porous layer on the hydrogen-charged Ti consists of anatase and rutile phases of TiO_2; it has the same chemical composition as the porous layer obtained on untreated Ti. X-ray photoelectron spectroscopy measurements show that prior hydrogen charging does not affect the thickness of anodic oxides on Ti. The porous oxide layer on Ti enables the growth of hydroxyapatite, thus revealing good bioactivity in simulated body fluids.

KEYWORDS: *titanium, porous layers, anodic oxidation, carrier density, biocompatibility*

INTRODUCTION

Titanium (Ti) and its alloys are widely used as biomedical materials and find application in the manufacture of artificial bones, dental and orthopedic implants, and others. This is because they have suitable chemical, physical, mechanical, and physiological properties. Their corrosion resistance in body fluids and biocompatibility with the human tissue make them excellent implant materials. In addition, Ti is a relatively light metal that possesses good ductility, high tensile modulus and fatigue strength, and a modulus of elasticity that matches that of the human bone. To improve the bone bonding ability of Ti implants, it is necessary to apply a suitable surface treatment.[1−14] For example, hydroxyapatite coatings are frequently applied to Ti orthopedic and dental implants because they facilitate tissue adhesion and ingrowth. The coatings are mainly formed by plasma spraying under high-temperature conditions,[4,5] though this can lead to changes in the crystal structure of the metal or alloy, reduced biocorrosion resistance, cracking of the coating, and other defects. Other coating methods, such as laser deposition,[6] sol–gel dipping,[7,8] electrophoresis,[9,10] and

Received: January 29, 2013
Accepted: March 14, 2013
Published: March 14, 2013

soaking in an alkaline solution[11−14] are also employed as suitable surface treatment procedures.

Although many techniques of Ti surface treatment are used for increasing its biocompatibility, electrochemical procedures are of particular interest because of their simplicity and low cost. For example, anodic oxidation is the most popular surface treatment which generates a protective film on aluminum, titanium, and valve metals. Since an anodic oxide film on Ti has a high electrical resistivity relative to the electrolyte and the bulk of Ti, the applied potential between Ti and an auxiliary electrode drops mainly across the anodic oxide film. The potential drop within the oxide gives rise to a high electric field that drives the migration of the Ti^{4+} and O^{2-} ions during the anodic oxide growth. As long as the electric field is strong enough to drive their migration, the growth of the anodic oxide film continues. There exists a linear relationship between the thickness of anodic oxide film and the applied anodic potential.[15] However, as the applied potential becomes high, the oxygen evolution reaction (OER) occurs concurrently with the formation of anodic oxide on Ti. Thus, the relationship between the oxide thickness and the applied potential is complex because several processes take place. A linear relationship is maintained for potentials lower than the dielectric breakdown limit of the anodic oxide, which is ca. 100 V, depending on electrolyte composition and other preparation conditions.[16] When the anodic potential is higher than the dielectric breakdown limit, the high electric field within the anodic oxide layer can trigger its electric breakdown and stimulate the formation of pores. Yang et al. reported that a porous layer on Ti was obtained when it was anodized in 1 M aqueous H_2SO_4 solution at a direct current voltage (V_{DC}) in the 90−180 V range.[17] They also reported that spark-discharge occurred during the anodization when the applied voltage was higher than 105 V. Interestingly, when the porous layer on Ti was formed in 1 M H_2SO_4 with spark-discharge and then employed as a biocompatible material by soaking in a simulated body fluid, apatite was observed to develop. On the other hand, no apatite was observed to develop when the anodic porous layer was grown without spark-discharge. Because the spark-discharge brings about structural changes to the surface of the Ti substrate and because the development of apatite on the Ti substrate is critical to its biocompatibility, it is necessary to optimize the method of preparing porous oxide layers on Ti without introducing any structural damage.

Shih et al. studied the influence of nanotitanium hydride on the formation of porous TiO_2 layers by anodization in 5 M aqueous NaOH solution.[18] The nanotitanium hydride was produced by cathodic polarization in 1 M aqueous H_2SO_4 before the anodization, and then a thick, anodic porous TiO_2 layer was formed. The authors suggested that the TiH_2 nanostructured phase present on Ti prior to anodization played an important role in the preparation of thick, porous TiO_2 layers. Similar results were reported by Tanaka et al. who demonstrated that a porous layer on the Ti was obtained upon immersion in a concentrated alkaline solution.[11−14] They indicated that hydrogen absorption and/or hydride formation during the immersion was a key factor in the preparation of a porous layer on Ti.

In this study, we report on the preparation of porous layers on Ti by anodization in 1 M H_2SO_4 at room temperature. We also examine the influence of cathodic treatment prior to anodization on the formation of porous TiO_2 layers with the objective of reducing the anodization potential and enhancing the porosity.

EXPERIMENTAL SECTION

Titanium Sample Preparation. The research involved the application of two types of Ti samples: wires and sheets. Ti wires were used in electrochemical measurements, and Ti sheets were used in all other experiments. Titanium wires (Nilaco Co., 99.5% in purity) of 0.5 mm in diameter and 10 cm long were used for the electrochemical measurements and scanning electron microscopy (SEM) characterization. Each specimen was degreased in acetone under reflux, dried in air, and eventually rinsed with ion exchange water (Millipore Milli-Q water purification system). Titanium sheets (Nilaco Co., 99.5% in purity) of 1.0 mm in thickness were used for grazing incident X-ray diffraction (GIXRD) measurements and X-ray photoelectron spectroscopy (XPS) analysis. They were cut to suitable dimensions, degreased in acetone under reflux, and then annealed to homogeneity at 1073 K for 4 h in a high vacuum furnace (high vacuum is required to eliminate the thermal formation of oxides, nitrides, carbides, or other compounds; the base pressure was maintained below 1.3×10^{-8} bar). Following the annealing, the specimens were first mechanically polished with 1200-grit SiC polishing paper and further polished to a smooth finish using diamond abrasives of various grades, the smallest being 1 μm. Subsequently, the specimens were treated with colloidal silica abrasives of various grades, the smallest being 0.04 μm, and degreased with acetone in an ultrasonic bath. The last treatment step yielded very smooth and shiny Ti specimens. The Ti sheet specimen was connected to a Ti wire by spot-welding (Kondo Technology Co., KTH-MWS) and covered with epoxy resin (Huntsman Advanced Materials Co., Araldite Rapid Type) except for the electrode area exposed to the electrolyte (analysis area = electrode geometric surface area). Finally, the specimens were etched in an aqueous mixture of HF (2% vol.) and HNO_3 (4% vol.) at room temperature for 5 s and then rinsed with ion exchange water. The geometric surface area of the Ti electrodes was determined using their dimensions.

Cathodic Treatment and Anodization of Ti. Titanium was cathodically polarized in 1 M aqueous H_2SO_4 solution before the anodization. The H_2SO_4 solution was prepared from analytical-grade chemicals (Kanto Chemical Co.) and ion exchange water (Millipore Milli-Q water). The solution temperature was kept constant at T = 303 K. A large platinum foil was used as a counter electrode. The cathodic treatment of Ti was conducted at a constant current density of j = 100 mA cm^{-2} for 10 min using a direct current (DC) power source (Takasago Ltd., model KX-100H). The distance between Ti and the counter electrode was kept constant at 30 mm. Subsequently, the polarity of the DC power source was reversed, and Ti was anodically oxidized at a constant voltage in the 90−150 V range for 1 min in the same electrolyte solution. After the anodization, the specimen was washed with ion exchange water and dried in air.

Materials Characterization. Materials characterization of the Ti surface at various stages of experiments was carried out using Ti sheet samples. Following electrochemical measurements, the specimens were rinsed with ion exchange water and carefully dried in air. The surface morphology was then examined using SEM (HITACHI Co., model S-2380N or ELIONIX Co., model ERA-8900FE), and the crystallographic structure was determined using GIXRD (PANalytical Co., model X'Pert PRO MRD). The incident angle of the X-ray beam was set at 1°, and the specimen was rotated during the measurement.

Electrochemical Measurements. Electrochemical measurements were conducted using a potentiostat (Hokuto Denko Co., model HA-501), a function generator (Hokuto Denko Co., model HB-104), and an A/D converter (DACS-Giken Co., model BX15W−H4); they were connected to a personal computer through a USB interface. Anodic potentiodynamic polarization curves were acquired at a scan sweep rate (s) of 0.1 V min^{-1}. During the acquisition of polarization curves, the aqueous H_2SO_4 solution was deaerated by bubbling Ar gas through the cell. The electrode potential was monitored using a reversible hydrogen electrode (RHE) immersed in the same electrolyte solution.

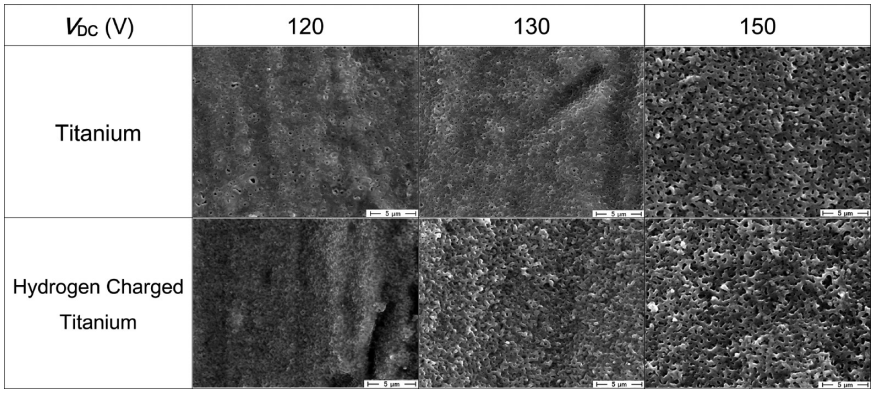

Figure 1. SEM micrographs of the surface of Ti after anodization for 1 min at various V_{DC} potentials in 1 M aqueous H_2SO_4 solution at T = 303 K without (first row) and with (second row) cathodic pretreatment.

Electrochemical impedance measurements were performed for anodized Ti electrodes in contact with deaerated 1 M aqueous H_2SO_4 solution at T = 303 K to determine the density of charge carriers in the anodic oxide film on Ti. A frequency response analyzer (NF Circuit Design Bloc Co., model S-5720C) combined with a potentiostat (Hokuto Denko Co., model HA-501) was employed. The measuring frequency was 1 kHz, and the potential amplitude was 10 mV. The impedance data were acquired using a personal computer connected through a GPIB interface. The electrochemical cell employed was a standard, all-glass, three-compartment one. The glassware was precleaned according to a well-established procedure described elsewhere.[19−21] During the electrochemical experiments, precleaned and presaturated with water vapor H_2 gas was bubbled through the reference electrode (RE) compartment in which a Pt electrode was immersed. A large platinum foil was used as a counter electrode. During the impedance measurements, the aqueous H_2SO_4 solution was deaerated by bubbling Ar gas through the cell.

Soaking in SBF. The biocompatibility of specimens was evaluated by the apatite-forming ability in simulated body fluid (SBF). The anodized titanium specimens were soaked in an SBF having an ion concentration equal to those of the human blood plasma at 309.5 K (Na^+ = 142.0, Ca^{2+} = 2.5, Mg^{2+} = 1.5, Cl^- = 147.8, HCO_3^- = 4.2, HPO_4^- = 1.0, and SO_4^{2-} = 0.5 mM). The SBF was prepared by dissolving reagent grade NaCl, $NaHCO_3$, KCl, $K_2HPO_4{\cdot}3H_2O$, $MgCl_2{\cdot}6H_2O$, $CaCl_2$, and Na_2SO_4 in ion exchange water according and adjusting its pH to 7.4 by adding with tris-hydroxymethylamino-methane $(CH_2OH)_3CNH_2$ and 1 M HCl; the solution was maintained at T = 309.5 K.[22] The temperature was kept constant by using a water bath. After being soaked for 336 h, the specimens were removed from SBF, washed gently with ion exchange water, and then dried in air at room temperature overnight. The apatite-forming ability was evaluated by the SEM observation of the surface of titanium after soaking in SBF for 336 h. The long soaking time employed in the course of the research was consistent with the procedure described elsewhere.[22]

RESULTS AND DISCUSSION

SEM Characterization. Figure 1 shows SEM micrographs of six Ti specimens after anodization at V_{DC} = 120, 130, and 150 V, respectively, in 1 M aqueous H_2SO_4 at T = 303 K without (first row) and with (second row) prior cathodic treatment. As is apparent from the first row in Figure 1, a porous layer on Ti starts to develop when the anodization potential is V_{DC} = 120 V. Increase of the potential to V_{DC} = 130 V increases the number of pores, but their size remains the same. However, the application of an anodization potential of 150 V generates a porous layer with a well-developed three-dimensional structure. Usually, the formation of anodized oxide film is driven by the migration of O^{2-} ions toward the inner metal/film interface and that of Ti^{4+} ions from metallic titanium to the outer film/electrolyte interface. During the anodization of Ti at a high anodic potential, the oxygen evolution proceeds vigorously on the Ti surface, and the specimen becomes surrounded by a layer of oxygen gas. Because the adjacent oxygen gas layer acts as an insulator, a high electric field is established between the Ti surface (including the oxide layer) and the gas layer. When the applied potential is above ca. 100 V, the gas layer cannot resist the electric field, and as a result, a spark-discharge takes place observed on the specimen damaging its surface; a dielectric breakdown of the oxide film proceeds under the same conditions. A high electric field also exists within the metal/film and film/electrolyte interfaces. If the oxide layer cannot resist such a high electric field, then it undergoes a dielectric breakdown producing pores in the oxide film. Because such dielectric discharges can happen at any location and at any time, numerous pores are created, and their assembly generates a porous, three-dimensional structure. Kuromoto et al. observed that the spark-discharge on anodized Ti and the formation of porous layer occurred simultaneously (at room temperature), when the applied voltage was higher than 100 V and the electrolyte was aqueous H_3PO_4 solution.[23] Teh et al. investigated the initial stage of anodic oxide growth on Ti in an alkaline pyrophosphate/aluminate electrolyte of commercial purity because of its relevance to plasma electrolytic oxidation of light metal alloy.[24] They suggested that the generation of molecular oxygen decreased the current efficiency of the anodic oxide growth and that oxygen nanobubbles were formed within the anodic film, resulting in the formation of cavities in the oxide film.

The second row in Figure 1 shows SEM micrographs of the Ti surface after anodization at V_{DC} = 120, 130, and 150 V in 1 M aqueous H_2SO_4 at T = 303 K but with prior cathodic treatment. They indicate that the porous layer starts to form on the Ti surface in the case of V_{DC} = 120 V and is already fully developed in the case of V_{DC} = 130 V. The middle images in the first and second row clearly illustrate the effect of prior cathodic treatment on the development of porous layer on Ti. The results demonstrate that the DC potential required to form a porous layer on Ti was significantly reduced, when the substrate was cathodically pretreated for 10 min in 1 M aqueous H_2SO_4. Thus, the cathodic treatment is observed to play an important role in reducing the DC potential needed to form an anodic porous layer. The decrease in V_{DC} as a result of the cathodic pretreatment also reduces the rate of oxygen gas evolution during the anodization. The reduced rate of oxygen evolution prevents the gaseous barrier layer from forming at the

substrate surface, thus inhibiting the spark-discharge from developing and reducing the possibility of Ti surface damage.

When Ti is cathodically polarized in 1 M aqueous H_2SO_4, the hydrogen evolution reaction (HER) proceeds; the overpotentially deposited H (H_{OPD}), which is a reaction intermediate, resides on the electrode surface (eq 1).[25−28] The adsorbed H_{OPD} has a certain residence time (lifetime) and can either become involved in the generation of H_2 through one of the two HER pathways depicted in eqs 2 and 2′ or undergo interfacial transfer to a subsurface state forming subsurface H (H_{ss}), eq 3. The H_{ss} species undergoes further transfer into the bulk of the host metal and becomes absorbed H (H_{abs}) (eq 4). Depending on the amount of H_{abs}, either a solid-state hydrogen solution (α phase) develops or a hydride precipitates (large amounts of H_{abs} give rise to the precipitation of Ti hydride in the form of needles that can be detected using optical microscopy).

$$H_2O + e^- \rightarrow H_{OPD} + OH^- \quad (1)$$

$$H_{OPD} + H_2O + e^- \rightarrow H_2 \uparrow + OH^- \quad (2)$$

$$H_{OPD} + H_{OPD} \rightarrow H_2\uparrow \quad (2')$$

$$H_{OPD} \rightarrow H_{ss} \quad (3)$$

$$H_{ss} \rightarrow H_{abs} \quad (4)$$

Titanium is a transition metal that easily oxidizes under gas-phase (in the presence of O_2(g) and at a high temperature) and electrochemical (e.g., upon the application of high DC voltage) conditions yielding in most cases TiO_2. The enthalpy of formation of TiO_2(s) is $\Delta_f H°(TiO_2) = -944.7$ kJ mol^{-1}; its value indicates that TiO_2(s) is a very stable compound.[29] Therefore, a freshly prepared metallic Ti specimen prepared by chemical etching spontaneously forms an oxide layer upon contact with air, water, or other oxidizing media, and its color changes from brilliant gray to dull gray. Elsewhere, it was proposed that an oxide layer on Ti having the TiO_2 chemical composition acts as a barrier to H absorption.[30,31] However, Ohtsuka et al. reported that under the conditions of electrolytic H_2 generation H atoms can penetrate the TiO_2 layer, initially transforming a Ti oxide into a hydroxide and eventually reaching the underlying Ti substrate and forming a hydride.[32] In addition, Azumi et al. studied the absorption of H into Ti using resistometry and indicated that an anodic oxide layer did not block hydrogen absorption when the Ti was cathodically polarized in the potential region corresponding to HER (those authors also used an aqueous H_2SO_4 solution).[33]

GIXRD Characterization. To examine whether there was any H_{abs} in the Ti substrate that had been pretreated cathodically in 1 M aqueous H_2SO_4, we performed GIXRD measurements on chemically etched Ti (the diffraction pattern (a) in Figure 2) and cathodically treated Ti (the diffraction pattern (b) in Figure 2). Our results demonstrate that the chemically etched Ti is free of any oxide layer that would give rise to a diffraction pattern. However, the freshly etched Ti is most likely covered with a nanoscopic layer of TiO_2 because its surface is very reactive. Such a layer cannot be detected using GIXRD because it is not a surface-sensitive technique. The results presented in Figure 2 (the diffraction pattern (b)) reveal the presence of a crystalline TiH_2 phase in the near-surface region of the cathodically pretreated Ti. Our GIXRD results are corroborated by transmission electron microscopy (TEM) experiments of Shih et al. who reported similar results.[18] Thus,

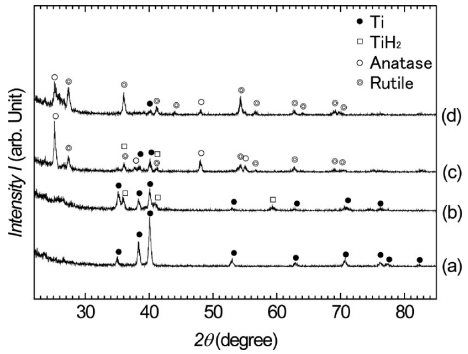

Figure 2. GIXRD diffraction patterns of the surface of untreated Ti (a), the hydrogen-charged Ti (b), the anodized Ti at V_{DC} = 130 V for 1 min with prior cathodic treatment (c), and the anodized Ti at V_{DC} = 150 V for 1 min (d). The X-ray incidence angle is 1°.

the results of GIXRD and TEM measurements are in good agreement. When Ti was charged with hydrogen by cathodic pretreatment and then anodized at V_{DC} = 130 V, a porous oxide layer developed (Figure 1). The GIXRD results (the diffraction pattern (c) in Figure 2) reveal the presence of two crystalline phases, namely, anatase and rutile. When Ti was anodized at 150 V but without any prior cathodic treatment, the rutile and anatase phases were also detected (the diffraction pattern (d) in Figure 2). Yang et al. investigated the formation of porous oxide layers on Ti by anodic oxidation in 1 M aqueous H_2SO_4 and reported that such layers were formed when V_{DC} was in the 90−180 V range and that the process was accompanied by spark-discharge.[17] They also reported that when the DC voltage was 155 V both anatase and rutile phases were obtained. However, when the DC voltage was 180 V, only the rutile phased developed. Our results and the finding of Yang et al.[17] suggest that the cathodic pretreatment has no impact on the crystallographic structure of the oxide that develops on Ti during the subsequent anodization. However, the presence of a hydride layer reduces the DC voltage required for the formation of a porous layer, thus minimizing the chance of sample damage due to spark-discharge.

XPS Characterization. The thickness of passive layers on Ti is known to depend on the magnitude of the applied voltage[34] in addition to the electrolyte composition and concentration, oxidation time, and temperature. However, it is unclear whether any cathodic pretreatment that generates a hydride layer affects the thickness of the TiO_2 layer that develops upon the subsequent anodization. To investigate the impact of TiH_2 on the formation of porous TiO_2, we prepared two identical TiO_2 layers by applying V_{DC} = 40 V, one without and the other with cathodic pretreatment. Subsequently, we examined their thickness using XPS and Ar-ion depth profiling; each Ar-ion sputtering cycle lasted 30 s, and right afterward an XPS spectrum was acquired. We examined the composition of the oxide layers by analyzing the intensities of the Ti($2p_{3/2}$) and O(1s) bands; there were no other elements detected within the oxide layer on Ti (traces of impurities that originated from the sample transfer via air disappeared after one Ar sputtering cycles). We also examined the time required for the O(1s) signal to drop to zero and for the Ti($2p_{3/2}$) signal to reach its maximum intensity. Figure 3 presents the atomic concentration of Ti and O in percentage as a function of the sputtering time. We observe that both XPS depth profiles have the same shape and the same chemical compositions at the zero sputtering

dx.doi.org/10.1021/am400398d | ACS Appl. Mater. Interfaces 2013, 5, 3340−3347

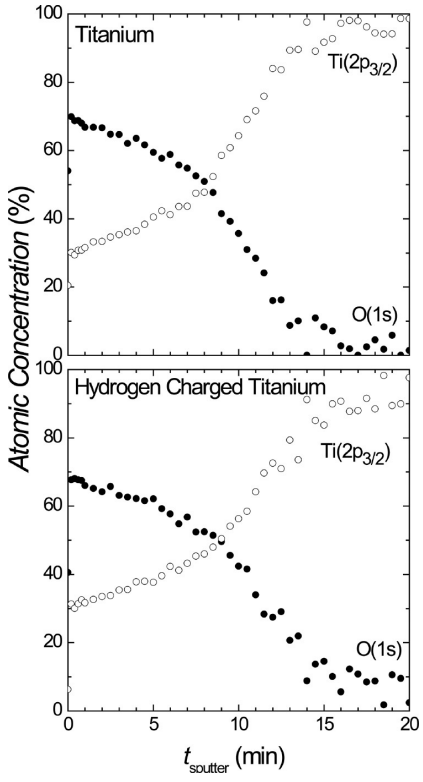

Figure 3. Composition depth profile of the TiO_2 layer on Ti (upper graph) and hydrogen-charged Ti (lower graph) expressed as atomic concentrations of O(1s) and metallic Ti($2p_{3/2}$) bands determined by XPS measurements. Anodization is conducted in 1 M aqueous H_2SO_4 at V_{DC} = 40.0 V for 1 min.

time. In both cases, the intensity of the O(1s) signal drops to zero, and the intensity of the Ti($2p_{3/2}$) signal levels off and reaches a maximum values after 15 ± 1 min of sputtering. The sputtering conditions produce a sputter rate of 12.8 nm min^{-1} for SiO_2 on top of Si. However, SiO_2 and TiO_2 have different sputter yields and sputter rates, thus it is impossible to deduce the thickness of the Ti oxide layers. Nevertheless, we may conclude that the two oxide layers have the same thickness. In addition, we may conclude that the cathodic pretreatment has no impact on the oxide layer thickness.

Mott–Schottky Measurements. We used a Mott–Schottky plot to examine the nature of the charge carriers and their density in the TiO_2 layer being in contact with deaerated 1 M aqueous H_2SO_4. The approach involved measuring the capacitance of the space charge region (C_{sc}) as a function of the electrode potential (E) under depletion conditions and employed the following relationship

$$\frac{1}{C_{sc}^{\ 2}} = \left(\frac{2N_A}{FN_D\varepsilon_r\varepsilon_o}\right)\left(E - E_{FB} - \frac{RT}{F}\right) \quad (5)$$

where E is the applied potential; E_{FB} is the flat band potential; F is the Faraday constant; N_A is the Avogadoro number; N_D is the charge carrier density (electron donor concentration for an n-type TiO_2); ε_r = 60 is the relative permittivity (dielectric constant) of TiO_2;[35–37] ε_o is the vacuum permittivity (dielectric constant); and RT/F is a temperature-dependent term and equals 0.0261 V at T = 303 K. It should be noted that the model is based on two assumptions: (i) the contribution of the double layer capacitance to the total capacitance (C_{dl}) is negligible, as C_{sc} is much smaller than C_{dl}, and (ii) the TiO_2 surface behaves ideally, and there is no contribution from surface states. Figure 4A presents two Mott–Schottky plots

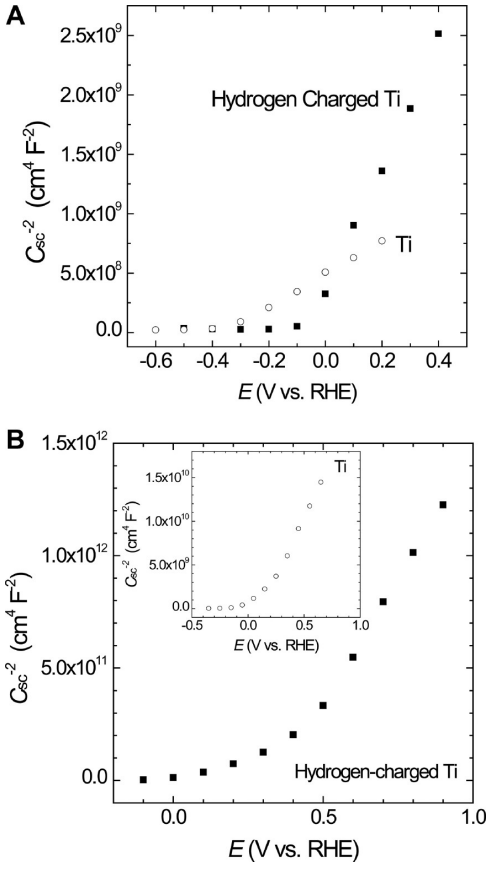

Figure 4. (A) Mott–Schottky plots for a native oxide layer on untreated Ti (open circles) and hydrogen-charged Ti (filled circles). Capacitance was measured at a single frequency of 1 kHz. (B) Mott–Schottky plots for an anodic oxide layer on untreated Ti (open circles) and hydrogen-charged Ti (filled circles). The anodic oxide layer was formed by applying V_{DC} = 10 V in 1 M aqueous H_2SO_4 for 60 s at T = 303 K. Capacitance was measured at a single frequency of 1 kHz.

measured at a single frequency of 1 kHz for: (i) Ti covered with a native oxide that develops upon contact with the surroundings (open circles) and (ii) hydrogen-charged Ti covered with a native oxide (filled circles); the cathodic pretreatment was carried out at a current density of j = 100 mA cm^{-2} for 30 min at T = 303 K. The experimental uncertainty of the C_{cs}^{-2} values reported in Figure 4A is ca. 3%. The results demonstrate that in the case of the native layer on Ti without any cathodic pretreatment C_{sc}^{-2} is initially zero and then starts increasing linearly when E is ca. −0.40 ± 0.02 V and reaches a value of ca. 7.5 × 10^8 ± 3.0 × 10^7 cm^4 F^{-2} for E = 0.20 V. In the case of the native layer formed on hydrogen-charged Ti, C_{sc}^{-2} is also initially zero and starts increasing linearly when E is ca. −0.1 ± 0.005 V and reaches a value of ca. 2.2 × 10^9 ± 8.8 × 10^7 cm^4 F^{-2} for E = 0.40 ± 0.02 V. In the case of the cathodically pretreated Ti, the C_{sc}^{-2} versus E plot has a greater slope than the one for untreated Ti. Fitting of the experimental results using a linear relationship allowed us to determine accurately the potential at which C_{sc}^{-2} = 0; this potential value corresponds to $E_{FB} - RT/F$ = 0, from which the value of E_{FB} can be calculated. We determined that E_{FB} = −0.36 ± 0.02 V for the native oxide on untreated Ti and E_{FB} = −0.04 ± 0.002 V

dx.doi.org/10.1021/am400398d | ACS Appl. Mater. Interfaces 2013, 5, 3340–3347

for the native oxide on hydrogen-charged Ti. At $E > E_{FB}$, the linear plots have a positive slope over the entire potential range studied implying that in both cases the native oxide layers have n-type semiconducting properties. This is an important observation because it demonstrates that the cathodic pretreatment has no impact on the type of semiconducting properties that the native oxide layers possess. The slope of the C_{sc}^{-2} versus E plots allows determination of the value of N_D. Because the slope equals $2N_A/FN_D\varepsilon\varepsilon_o$ (eq 5), a steeper plot corresponds to a lower value of N_D. We determined that $N_D = 1.5 \times 10^{21} \pm 6.0 \times 10^{19}$ cm^{-3} for the native oxide on untreated Ti, and $N_D = 4.2 \times 10^{20} \pm 1.7 \times 10^{19}$ cm^{-3} for the native oxide on cathodically pretreated Ti. The results reveal that the prior cathodic treatment reduces the number of charge carriers by a factor of ca. 3.5. Because the charge carrier density is usually related to the crystallinity of the species, here TiO_2,[38,39] the results suggest that the oxide layer on the cathodically charged Ti is more organized and compact than that on untreated Ti. We also investigated the electronic properties of a TiO_2 layer developed by applying $V_{DC} = 10$ V on untreated and hydrogen-charged Ti by recording Mott–Schottky plots. The results presented in Figure 4B (the experimental uncertainty of the C_{cs}^{-2} values reported in Figure 4B is ca. 3%) reveal that these plots also have a positive slope pointing to an n-type semiconducting nature of the TiO_2 layer. In the case of the anodically formed TiO_2 on Ti without any cathodic pretreatment, C_{sc}^{-2} is initially zero and then starts increasing linearly when E is ca. -0.05 ± 0.0025 V and reaches a value of ca. $1.5 \times 10^{10} \pm 6.0 \times 10^8$ cm^4 F^{-2} for $E = 0.65 \pm 0.032$ V. In the case of the TiO_2 layer formed on Ti with cathodic pretreatment, C_{sc}^{-2} is also initially zero and starts increasing linearly when E is ca. 0.0 V and reaches a value of ca. $1.2 \times 10^{12} \times 4.8 \times 10^{10}$ cm^4 F^{-2} for $E = 0.90 \pm 0.045$ V. Fitting of the experimental results using a linear relationship allowed us to determine accurately the potential at which $C_{sc}^{-2} = 0$; this potential value corresponds to $E_{FB} - RT/F = 0$, from which the value of E_{FB} can be calculated. By adopting this approach, we determined that $E_{FB} = 0.14 \pm 0.07$ V for the anodic oxide on untreated Ti and $E_{FB} = 0.35 \pm 0.018$ V for the native oxide on hydrogen-charged Ti. At $E > E_{FB}$, the linear plots have a positive slope over the entire potential range studied, implying that in both cases the native oxide layers are n-type semiconductors. The slopes of the C_{sc}^{-2} vs E plots allow the determination of the value of N_D that is $8.6 \times 10^{19} \pm 3.4 \times 10^{18}$ cm^{-3} for the anodic oxide layer on untreated Ti and $1.1 \times 10^{18} \pm 4.4 \times 10^{16}$ cm^{-3} for the anodic oxide layer on hydrogen-charged Ti. All values of N_D and E_{FB} are summarized in Tables 1 and 2, respectively. The analysis of Mott–Schottky measurements is based on the assumption that the contribution of C_{dl} to C_{sc} is negligible. This assumption is valid only in the case of oxide layers having low porosity because C_{dl} may not be assumed to be negligible in the case of highly porous materials. This is the main reason why Mott–Schottky measurements were performed on oxide layers formed at $V_{DC} = 10$ V.

Table 1. Values of Charge Carrier Density (N_D in cm^{-3}) for Ti and TiO_2 Layers on Untreated and Hydrogen-Charged Samples

V_{DC} [V]	untreated Ti	hydrogen charged Ti
0	$1.5 \times 10^{21} \pm 6.0 \times 10^{19}$	$4.2 \times 10^{20} \pm 1.7 \times 10^{19}$
10	$8.6 \times 10^{19} \pm 3.4 \times 10^{18}$	$1.1 \times 10^{18} \pm 4.4 \times 10^{16}$

Table 2. Values of Flat Band Potential (E_{FB} in V) for Ti and TiO_2 Layers on Untreated and Hydrogen-Charged Samples

V_{DC} [V]	untreated Ti	hydrogen charged Ti
0	-0.36 ± 0.02	-0.04 ± 0.002
10	0.14 ± 0.007	0.35 ± 0.018

An analysis of the values of N_D and E_{FB} allows us to identify the following similarities and trends: (i) the native oxides and anodic oxides on Ti are n-type semiconductors; (ii) both hydrogen charging and anodization reduce the value of N_D; (iii) N_D has the highest value for untreated Ti that is covered only with a thin layer of native oxide; and (iv) N_D has the lowest value for hydrogen-charged and anodic layer-covered Ti. The latter observation is consistent with the results reported elsewhere, indicating that an increase in thickness of an anodic oxide layer through rise of the anodization potential and/or anodization time decreases the value of N_D.[38,39]

It is necessary to explain the decrease in N_D brought about by hydrogen charging and anodic oxide formation. The charge carriers in TiO_2 are oxygen atom vacancies, and consequently, the value of N_D depends on their number. In addition, the value of N_D also depends on the degree of crystallinity within an oxide layer, and in general, the higher the degree of crystallinity, the lower the value of N_D. The native oxide layer on Ti is amorphous in nature, while the anodically formed oxide layers are crystalline (anatase and rutile). Consequently, a native oxide layer is expected to have a greater value of N_D than an anodic oxide film, and our experimental values of N_D reported in Table 1 meet this expectation. It is also necessary to explain why hydrogen charging decreases the value of N_D in the case of native and anodic oxides, although it does not affect the oxide layer thickness as may be concluded on the basis of our XPS measurements. At this preliminary stage, interpretation of our N_D values leads to the suggestion that oxide layers on hydrogen-charged Ti have a greater degree of crystallinity (organization), but additional research is needed to verify the validity of this proposal. We relate this behavior to the existence of a crystalline Ti hydride phase (see GIXRD Characterization) on which the native oxide or anodic oxide subsequently develops.

Schematics of the Oxide Growth. Figure 5 shows a schematic diagram of the oxide growth behavior on untreated (left-hand diagram) and hydrogen-charged (right-hand diagram) Ti in aqueous H_2SO_4 solution upon application of a DC voltage; the arbitrary potential scale is the same for the two types of samples. In the case of untreated Ti, the oxide layer thickness increases as the applied voltage (V_{app}) is raised (for all other parameters being constant), and the greater the applied voltage the thicker the oxide layer. The current flow is facilitated by charge carriers that are related to structural defects. Because there are many charge carriers, the applied DC voltage does not create conditions that would trigger an electric breakdown of the oxide later. However, the adjacent oxygen layer creates favorable conditions for spark-discharge, and as spark-discharge occurs, a porous layer develops. In the case of the hydrogen-charged Ti, the thickness of the anodic layer also increases as V_{app} is raised (for all other parameters being constant). However, the oxide layer on hydrogen-charged Ti has a lower density of charge carriers (Table 1), thus higher resistivity. Consequently, the same V_{app} that does not trigger any electric breakdown in the case of untreated Ti triggers electric breakdown of the anodic oxide layer in the case of hydrogen-charged Ti; the electrical breakdown is accompanied

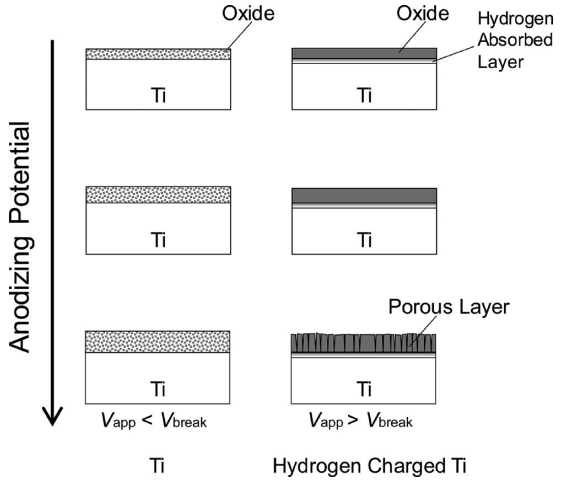

Figure 5. Schematic visualization of the mechanism of porous anodic oxide formation in aqueous H_2SO_4 by anodization on untreated Ti (left-had diagram) and hydrogen-charged Ti (right-hand diagram).

by the development of a porous layer. The novel aspect of this research is that a lower DC voltage can be effectively applied to develop a porous oxide layer on Ti, but the substrate required prior hydrogen charging.

Corrosion Behavior in Simulated Body Fluids. The bioactivity of artificial materials is typically evaluated by the formation of a biologically active, bone-like carbonate containing hydroxyapatite in a simulated body fluid (SBF).[22] To evaluate the bioactivity of our anodically formed porous layers on Ti, we soaked the anodized Ti specimens in SBF for 336 h at T = 309.5 K. Figure 6 shows SEM photographs of the surface of untreated and anodized Ti (upper image) and hydrogen-charged and anodized Ti (lower image) following their immersion in SBF. We observe the precipitation of apatite

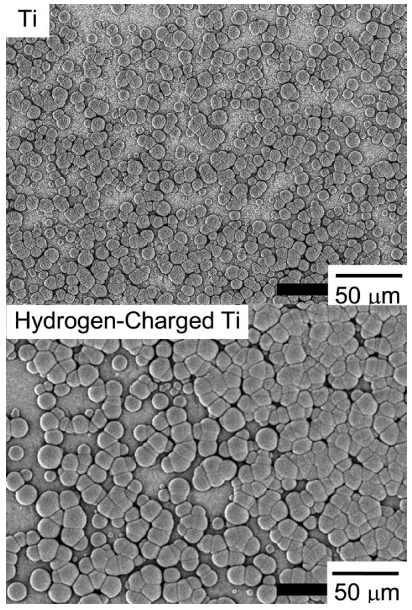

Figure 6. SEM micrographs of the surface for the oxide layer on untreated Ti (upper image) and hydrogen-charged Ti (lower image) after immersion in a simulated body fluid solution at T = 309.5 K for 336 h. The anodic oxide was formed by applying V_{DC} = 150 V for 1 min in 1 M aqueous H_2SO_4.

on the surface of Ti (it gives rise to "bubble-like" surface features) irrespective of the hydrogen charging. The SEM images also demonstrate that the size of these "bubble-like" features is larger in the case of hydrogen-charged Ti than in the case of untreated Ti. These results imply that the hydroxyapatite formation on the porous oxide on hydrogen-charged Ti is easier as compared to untreated Ti. It is well established that the rate of precipitation of hydroxyapatite on the surface of Ti strongly depends on the number of Ti−OH groups that can be obtained by chemical treatment.[40] The surface hydroxyl groups, such as SiOH, TiOH, etc., are known to act as effective promoters of apatite nucleation.[41,42] Depending on the medium's pH, the Ti−OH groups can have positive or negative charges.[43] We propose the following mechanism of the precipitation of hydroxyapatite on the anodically formed porous oxide layer on Ti. In the case of SBF, the Ti−OH groups carry negative charges, which then attract Ca^{2+} cations through electrostatic interactions.[44] Subsequently, HPO_4^{2-} anions undergo adsorption, effectively giving rise to the precipitation of apatite crystals.[44] Because the amount of hydroxyapatite that develops on Ti oxide depends on its porosity, the magnitude of V_{DC} and the prior hydrogen charging indirectly impact the porous layers' biocompatibility. Because we do not know the number of Ti−OH groups on the surface of porous oxide layers, we limit our discussion to a qualitative interpretation. The results presented in Figure 6 suggest that prior hydrogen-charging increases the ability of a porous, anodic oxide to develop a bioactive, hydroxyapatite deposit. However, further research is needed to investigate the formation mechanism of porous oxide on Ti and to evaluate their biocompatibility.

CONCLUSIONS

To decrease the anodization voltage required to form porous oxide layers on Ti, we investigated the influence of prior hydrogen charging on the development of porous anodic oxides. The main conclusion and new findings are summarized as follows: (i) microporous layer on Ti can be prepared by anodization with spark-discharge in a 1 M aqueous H_2SO_4 solution at 303 K but can also be obtained without spark-discharge in the same electrolyte using hydrogen-charged Ti; (ii) the charge carrier density in anodic oxide on hydrogen-charged Ti is lower than that in anodic oxide on untreated Ti; (iii) porous anodic oxides on Ti facilitate the formation of hydroxyapatite in a simulated body fluid irrespective of prior hydrogen charging; and (iv) the growth of the hydroxyapatite layer on a porous, anodic oxide on Ti is easier if the Ti substrate has been charged with hydrogen prior to the oxide growth.

AUTHOR INFORMATION

Corresponding Author

*E-mail: s-tanaka@kurume-nct.ac.jp; gregory.jerkiewicz@chem.queensu.ca.

Notes

The authors declare no competing financial interest.

ACKNOWLEDGMENTS

Grateful acknowledgement is made to the Japan Society for the Promotion of Science (JSPS), Grant-in-Aid for Scientific Research (C), No.24550241. We wish to acknowledge the Light Metal Educational Foundation, Inc. for providing

financial support. We acknowledge financial support from the Natural Sciences and Engineering Research Council of Canada through the Discovery Grant, Research Tools and Instruments Grant, and Strategic Grant programs. We acknowledge financial support from The Foundation for Applied Research and Technological Uniqueness at Nagaoka University of Technology. We thank Kurume National College of Technology and Queen's University for providing financial support to carry out this project.

REFERENCES

(1) Kim, H.-M.; Miyaji, F.; Kokubo, T.; Nakamura, T. *J. Ceram. Soc. Jpn.* **1997**, *105*, 111−116.
(2) Kim, H.-M.; Miyaji, F.; Kokubo, T.; Nishiguchi, S.; Nakamura, T. *J. Biomed. Mater. Res.* **1999**, *45*, 100−107.
(3) Kim, H.-M.; Miyaji, F.; Kokubo, T.; Nakamura, T. *J. Mater. Sci.: Mater. Med.* **1997**, *8*, 341−347.
(4) Ducheyne, P.; Van Raemdonck, W.; Heughebaert, J. C.; Heughebaert, M. *Biomaterials* **1986**, *7*, 97−103.
(5) Thomas, K. A.; Kay, J. F.; Cook, S. D.; Jarcho, M. *J. Biomed. Mater. Res.* **1987**, *21*, 1395−1414.
(6) Bagratashvili, V. N.; Antonov, E. N.; Sobol, E. N.; Popov, V. K.; Howdle, S. M. *Appl. Phys. Lett.* **1995**, *66*, 2451−2453.
(7) Lee, J.; Aoki, H. *Bio-Med. Mater. Eng.* **1995**, *5*, 49−58.
(8) Li, P.; Groot, K.; Kokubo, T. *J. Sol-Gel Sci. Technol.* **1996**, *7*, 27−34.
(9) Ducheyne, P.; Radin, S.; Heughebaert, M.; Heughebaert, J. C. *Biomaterials* **1990**, *11*, 244−254.
(10) Gottlander, M.; Johansson, C. B.; Wennerberg, A.; Albrektsson, T.; Radin, S.; Ducheyne, P. *Biomaterials* **1997**, *18*, 551−557.
(11) Tanaka, S.; Aonuma, M.; Hirose, N.; Tanaki, T. *J. Electrochem. Soc.* **2002**, *149*, D167−D171.
(12) Tanaka, S.; Iwatani, T.; Hirose, N.; Tanaki, T. *J. Electrochem. Soc.* **2002**, *149*, F186−F190.
(13) Tanaka, S.; Hirose, N.; Tanaki, T. *J. Electrochem. Soc.* **2005**, *152*, C789−C794.
(14) Tanaka, S.; Tobinatsu, H.; Maruyama, Y.; Tanaki, T.; Jerkiewicz, G. *ACS Appl. Mater. Interfaces* **2009**, *1*, 2312−2319.
(15) Ohtsuka, T.; Nomura, N. *Corros. Sci.* **1997**, *39*, 1253−1263.
(16) Kim, K.-H.; Ramaswamy, N. *Dent. Mater. J.* **2009**, *28*, 20−36.
(17) Yang, B.; Uchida, M.; Kim, H.-M.; Zhang, X.; Kokubo, T. *Biomaterials* **2004**, *25*, 1003−1010.
(18) Shih, Y.-H.; Lin, C.-T.; Liu, C.-M.; Chen, C.-C.; Chen, C.-S.; Ou, K.-L. *Appl. Surf. Sci.* **2007**, *253*, 3678−3682.
(19) Angerstein-Kozlowska, H.; Conway, B. E.; Sharp, W. B. A. *J. Electroanal. Chem.* **1973**, *43*, 9−36.
(20) Angerstein-Kozlowska, H. In *Comprehensiue Treatise of Electrochemistry*; Yeager, E., Bockris, J. O'M., Conway, B. E., Sarangapani, S., Eds.; Plenum Press: New York, 1984; Vol. *9*, Chapter 9.
(21) Conway, B. E.; Sharp, W. B. A.; Angerstein-Kozlowska, H.; Criddle, E. E. *Anal. Chem.* **1973**, *46*, 1321−1336.
(22) Kokubo, T.; Takadama, H. *Biomaterials* **2006**, *27*, 2907−2915.
(23) Kuromoto, N. K.; Simão, R. A.; Soares, G. A. *Mater. Charact.* **2007**, *58*, 114−121.
(24) Teh, T. H.; Berkani, A.; Mato, S.; Skeldon, P.; Thompson, G. H.; Habazaki, H.; Shimizu, K. *Corros. Sci.* **2003**, *45*, 2757−2768.
(25) Conway, B. E.; Jerkiewicz, G. *Z. Phys. Chem.* **1994**, *183*, 281−286.
(26) Jerkiewicz, G.; Zolfaghari, A. *J. Electrochem. Soc.* **1996**, *143*, 1240−1248.
(27) Jerkiewicz, G. *Prog. Surf. Sci.* **1998**, *57*, 137−186.
(28) Qian, S. Y.; Conway, B. E.; Jerkiewicz, G. *Int. J. Hydrogen Energy* **2000**, *25*, 539−550.
(29) Lide, D. R. *CRC Handbook of Chemistry and Physics*, 74th ed.; CRC Press: Boca Raton, FL, 1993.
(30) Shimogori, K. *Boshoku Gijutsu* **1998**, *30*, 349−357.
(31) Fukuzuka, T.; Shimogori, K.; Satoh, H.; Tomari, H. *Boshoku Gijutsu* **1979**, *28*, 379−385.
(32) Ohtsuka, T.; Masuda, M.; Seo, M. *J. Electrochem. Soc.* **1985**, *132*, 787−792.
(33) Azumi, K.; Asada, Y.; Ueno, T.; Seo, M.; Mizuno, T. *J. Electrochem. Soc.* **2002**, *149*, B422−B427.
(34) Jerkiewicz, G.; Strzelecki, H.; Wieckowski, A. *Langmuir* **1996**, *12*, 1005−1010.
(35) McAleer, J. F.; Peter, L. M. *Faraday Discuss.* **1980**, *70*, 67−80.
(36) Azumi, A.; Ohtsuka, T. *Zairyo to Kankyo* **1997**, *46*, 169−175.
(37) Azumi, K.; Seo, M. *Corros. Sci.* **2001**, *43*, 533−546.
(38) Azumi, A.; Ohtsuka, T. *Zairyo to Kankyo* **1997**, *46*, 384−390.
(39) Schultze, J. W.; Stimming, U.; Weise, J. *Ber. Bunsenges. Phys. Chem.* **1982**, *86*, 276−282.
(40) Xiao, F.; Tsuru, K.; Hayakawa, S.; Osaka, A. *Thin Solid Films* **2003**, *441*, 271−276.
(41) Kasuga, T.; Kondo, H.; Nogami, M. *J. Cryst. Growth* **2002**, *235*, 235−240.
(42) Kokubo, T.; Kim, H.-M.; Kawashita, M. *Biomaterials* **2003**, *24*, 2161−2175.
(43) Ma, Q.; Li, M.; Hu, Z.; Chen, Q.; Hu, W. *Mater. Lett.* **2008**, *62*, 3035−3038.
(44) Liang, F.; Zhou, L.; Wang, K. *Surf. Coat. Technol.* **2003**, *165*, 133−139.